ACS Sustainable Chemistry & Engineering

Research Article

pubs.acs.org/journal/ascecg

Mesoporous TiO_2 Single-Crystal Polyhedron-Constructed Core–Shell Microspheres: Anisotropic Etching and Photovoltaic Property

Meigui Xu, Peng Ruan, HaiXian Xie, Ang Yu, and Xingfu Zhou*

State Key Laboratory of Materials-Oriented Chemical Engineering, College of Chemistry and Chemical Engineering, Nanjing University of Technology, Nanjing 210009, P.R. China

ABSTRACT: A favorable micro-nanostructure is crucial for obtaining superior properties. However, the synthetic techniques for synthesizing the complex morphology still remain a challenge. In this work, we synthesized core–shell-structured submicrometer-sized mesoporous TiO_2 microspheres (MTMs) constructed with mesoporous TiO_2 polyhedrons through a novel anisotropic etching route. The outer shell of the obtained TiO_2 microsphere is constructed by a mesoporous TiO_2 single-crystal nanopolyhedron with exposed (101) facets. Hydrogen peroxide was used as the bubble generator, which simultaneously acted as gas templates for the formation of TiO_2 microspheres. Fluorine ions facilitate the formation of anatase (001) facets at the beginning of the reaction. The anisotropic etching accrued along the [101] direction with an increase in fluorine ions, leaving mesoporous structures and highly exposed (101) facets. Dye-sensitized solar cells (DSSCs), using the as-prepared product as a light-scatting layer, showed a 29.4% increase in conversion efficiency.

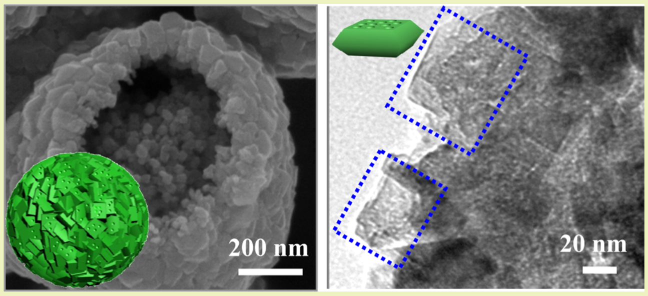

KEYWORDS: *Mesoporous TiO_2, Single crystal, Core–shell microspheres, Anisotropic etching, Dye-sensitized solar cells*

INTRODUCTION

Since the original work of Grätzel and co-workers in 1991, dye-sensitized solar cells (DSSCs) have been considered one of the most promising candidates for recycled energy devices because of their high energy conversion efficiencies and low production cost.[1−4] A typical DSSC device is structurally composed of a photoanode, a counter electrode of a photocathode, and an electrolyte. As the photoanode part, semiconductor metal oxides, such as TiO_2, ZnO, and WO_3, are extensively used.[5−9] Among these metal oxides, DSSCs based on TiO_2 have attracted much attention and have shown excellent performance in DSSC devices due to their strong affinity to dye molecules and high chemical stability.[10] The performance of the DSSCs is greatly affected by the morphology and structure of the titania used in the photoanodes. Nanostructured TiO_2 materials have been widely applied to dye-sensitized solar cells as the photoactive layer in nanorods,[11−13] nanotubes,[14−16] nanowires,[17−19] and nanoparticles.[20−22] Among those TiO_2 structures, three-dimensional (3-D) TiO_2 is a promising structure for improving the performance of DSSCs due to its light-scattering effects. It is reported that optimizing the 3-D structure of TiO_2 with a suitable submicrometer size can greatly enhance its light-scattering effects.[23,24]

The performance of the DSSCs based on TiO_2 is also affected by the crystalline phase. It is well known that anatase, rutile, and brookite are the most common polymorphs of titania. Anatase TiO_2 with a tetragonal structure (the *c*-axis being 2.7 times the *a*-axis) is one of the most important semiconductors, playing a central role in photovoltaic cells because of its surface chemistry and higher Fermi level.[25,26] For anatase TiO_2, the (101) facet has a lower surface energy of 0.44 J m^{-2} than other two facets, (100) (0.53 J m^{-2}) and (001) (0.90 J m^{-2}).[27] Under equilibrium conditions, the natural and synthetic anatase TiO_2 single crystals mainly exist with a morphology of an octahedral bipyramid, in which the majority of the surface is normally enclosed by energetically favorable (101) facets rather than the more reactive (001) facets.[28] Anatase (101) surfaces with low energy have a strong ability to absorb a (COOH) group[29] and, thereby, can enhance the combination of dye molecules and TiO_2 nanoparticles. The highly exposed (101) facet is favorable for improving energy conversion efficiency. Furthermore, mesoporosity provides the desired highly accessible surfaces, and single-crystal semiconductors have long-range electronic connectivity and structural coherence. However, it is difficult to obtain mesoporous single crystals. Recently, Snaith et al. reported for the first time the fabrication of mesoporous TiO_2 single crystal by using mesoporous SiO_2 as a hard template.[30] However, it still remains a major challenge to successfully synthesize mesoporous TiO_2 single crystals with a designed crystalline facet and a suitable submicrometer size for enhancing light scattering.

In our previous work,[31] we reported the first use of the anisotropic corrosion strategy to fabricate rutile TiO_2 nano-

Received: July 31, 2013
Revised: February 18, 2014
Published: February 24, 2014

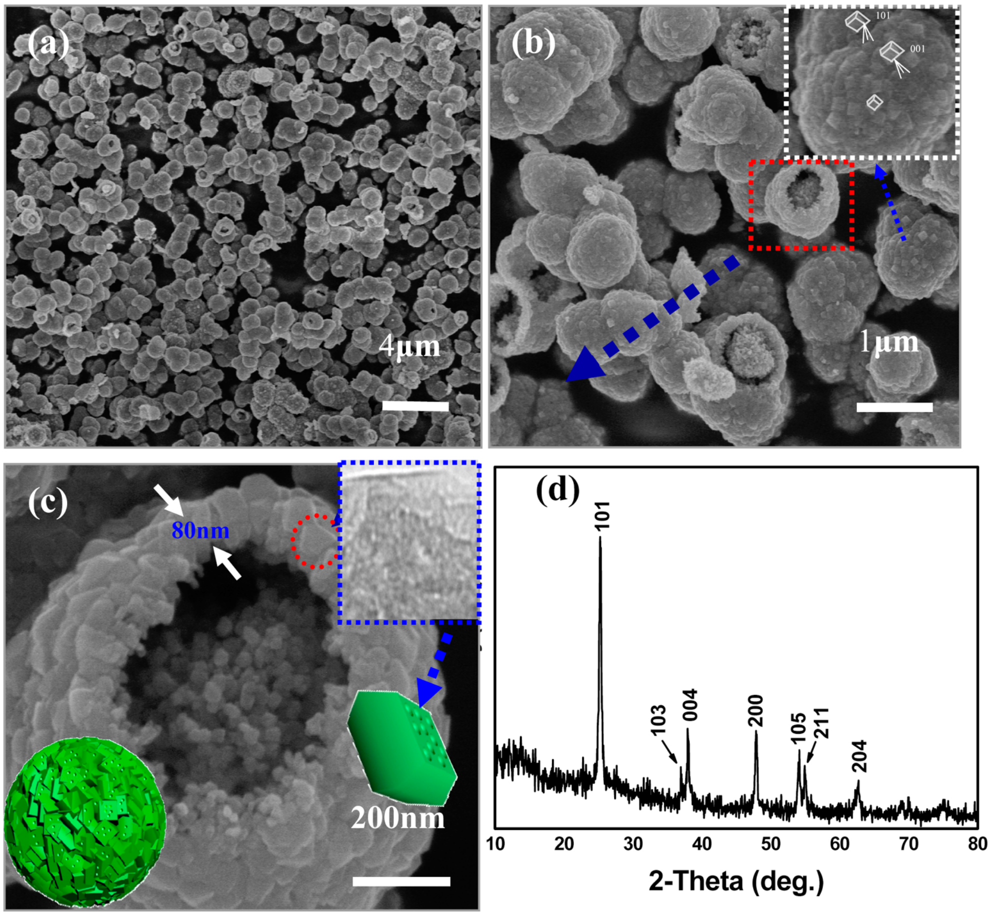

Figure 1. (a) FESEM overview of as-synthesized products. (b) Higher magnification FESEM image of as-obtained core−shell-structured TiO_2 MTMs. (c) SEM image of an individual cracked TiO_2 microsphere, showing the core−shell structure. Top right is the HRTEM of the mesoporous TiO_2 nanoparticles building block. Bottom left is the cartoon of the TiO_2 microsphere. (d) XRD patterns of as-prepared MTMs.

tubes with a tapered inner structure by the reaction of preformed rutile TiO_2 nanorods with hydrochloric acid under hydrothermal conditions. Here, we extend the anisotropic etching strategy to the preparation of core−shell-structured MTMs. The obtained microspheres are constructed by two components. The core is composed of TiO_2 nanoparticles, while the shell is composed of mesoporous TiO_2 single-crystal nanopolyhedra with highly exposed (101) facets. The submicrometer-sized MTMs can be applied as the light-scattering layer of the DSSCs. We use the as-prepared product to optimize the DSSCs. Because of the special mesoporous structures and the exposed (101) facets, the optimized DSSCs based on our as-prepared sample showed an overall light electron conversion efficiency of 6.64%, which is 27% higher than that of the DSSCs based on commercial P_{25}.

EXPERIMENTAL SECTION

All chemicals are analytical-grade regents without further purification. The TiO_2 precursor (tetrabutyl titanate hydrolysate) was first prepared for further synthesis procedure, and the method was described elsewhere.[32,33] A total of 4 mL of tetrabutyl titanate [$TiO(C_4H_9)_4$] was dissolved in 20 mL ethanol under stirring for 10 min, and then 60 mL of deionized water was added dropwise into the solution until no more white precipitate was produced. The white TiO_2 precursor was collected and washed with water several times and dried in air at 353 K. In our typical hydrothermal procedure, 20 mL of deionized water and 30 mL of H_2O_2 were first mixed, and then 0.2 g of as-prepared tetrabutyl titanate hydrolysate and 0.64 g of NH_4F was added into the mixed solution with constant stirring with a magnetic pulsator at room temperature for about 30 min. The mixture was transferred into a Teflon-lined stainless steel autoclave (80 mL capacity). The autoclave was heated and held at 453 K for 12 h and then allowed to cool to ambient temperature naturally. The product was collected and washed with water and ethanol several times and dried in air at 353 K. The powder was synthesized for preparing the anti-reflection layer electrode paste.

The morphology of the samples was obtained on a field emission scanning electron microscopy (FESEM, HITACHI S-4800), and high-resolution transmission electron microscopy was performed on a JEOL JEM-2010UHR instrument with an acceleration voltage of 200 KV. The obtained samples were characterized by powder X-ray diffraction (XRD) analyses, which were performed on a Bruker-D8Advance X-ray diffractometer with graphite monochromatized high-intensity Cu Kα radiation (λ = 1.5418 Å) at 40 KV and 30 mA. The XRD patterns were recorded from 10 to 80° (2θ) with a scanning step of 0.05° at a counting time of 0.2 s per step. The morphology of the as-synthesized TiO_2 was also observed using JEOL-2100 high-resolution transmission electron microscope (HRTEM) with an accelerating voltage of 200 kV, along with selected area electron diffraction (SAED) pattern. The surface area of the sample was measured by the Brunauer−Emmett−Teller (BET, Omnisorp100 cx, Coulter, U.S.A.) method.

Before the device fabrication, the obtained core−shell-structured MTM powder sample and Degussa P_{25} was pretreated by dispersing it in an ethanol solution containing ethyl cellulose and terpineol, followed by grinding in an agate mortar at room temperature for 30 min. The optimized device was prepared by screen printing using Deguass P_{25} TiO_2 as the photoactive layer and the obtained core−shell-structured MTM as the scattering layer. The prepared TiO_2 paste

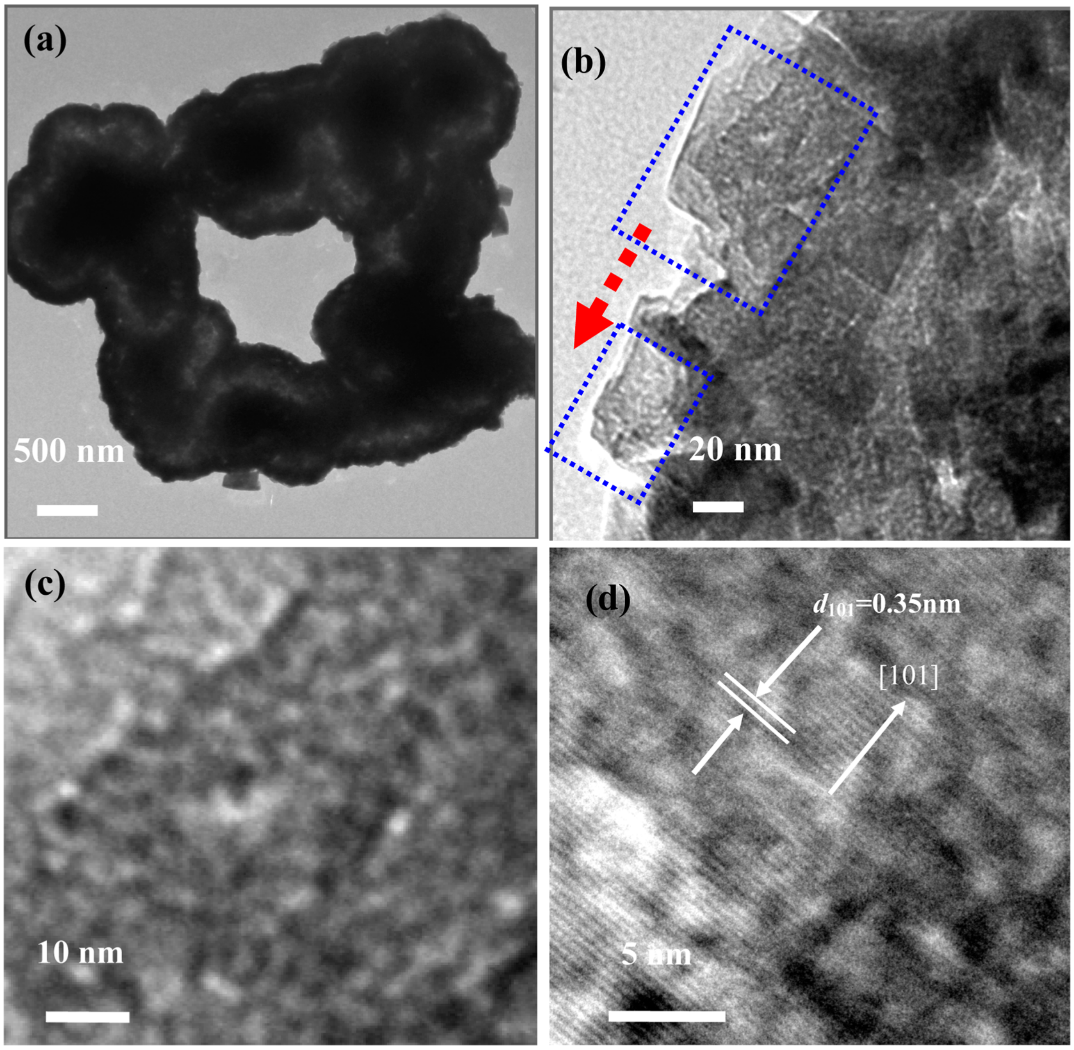

Figure 2. TEM and HRTEM images of the as-synthesized product: (a) TEM image of overall view of a core−shell MTM. (b) HR-TEM image of the TiO_2 polyhedra in the surface of the core−shell microsphere. (c) HRTEM image of the mesoporous structure of the polyhedra. (d) HRTEM image of the irregular mesoporous structure.

was coated onto the FTO glass (FTO, 14 Ω per square, Nippon Sheet Glass, Japan) layer using the screen print method. Before this step, the glass was treated with 40 mM $TiCl_4$ aqueous solution at 343 K for 30 min. The film was calcinated in a muffle furnace at 723 K for 30 min. After that, the film-coated glass was treated with 40 mM $TiCl_4$ aqueous solution at 343 K for 30 min and sintered at 723 K for 30 min again. We then allowed the fabricated TiO_2 films to cool to 353 K for dye adsorption. The fabricated TiO_2 films were immersed in anhydrous ethanol containing N719 dye (cis-bis(isothiocyanato)bis(2,2′-bipyr-ridyl-4−4′-dicarboxylato)-ruthenium(II)bis-tetrabutylammonium) and were kept for 24 h at room temperature. Later, the film was rinsed with pure ethanol to remove the physically adsorbed dye molecules and stored at 353 K under air conditions. For comparison, two other photoanodes based on Degussa P_{25} and the obtained core−shell-structured MTM powders were prepared in the same way as described above. The Pt-coated FTO, used as a counter electrode, was prepared by screen printing the H_2PtCl_6 solution on to a FTO glass followed by heating at 723 K for 15 min in air. Finally, the dye-adsorbed TiO_2 photoanode and Pt counter electrode were assembled into a sandwich-type cell and sealed with a hot melt gasket of 25 μm thickness made of theionomer Surlyn 1702 (Dupont). The electrolyte consisted of 1-butyl-3-methyl-imidazolium iodide (0.6M), guanidinium thiocyanate $I_{2,}$ and 4-tert-butylpyridine (0.5 M) in acetonitrile and valeronitrile (85:15 v/v). The active area of the dye-coated TiO_2 film was 0.16 cm^2.

Photocurrent−voltage measurements were performed using a Keithley 2420 source meter (Keithley, U.S.A.). A 450 W xenon lamp (Oriel, U.S.A.) was used as the light source, and the light intensity was AM 1.0 G one sun (100 mW/cm^2) calibrated with a standard Si solar cell. The active area of the tested solar cells was 0.16 cm^2. Electrochemical impedance spectroscopy (EIS) was measured by applying bias of the open circuit voltage under 100 mW cm^{-2} light illumination by a computer-controlled electrochemical workstation (CHI 660C, CH Instruments) in a frequency range from 100 to 10^5 Hz with an alternating current amplitude of 5 mV. The diffuse reflectance spectra of the TiO_2 films were recorded by a Perkin-Elmer UV−vis spectrophotometer (model Lambda 950). In order to calculate the amount of dye in the TiO_2 electrode, we immersed the dye-adsorbed TiO_2 films with a size of 1 cm^2 into a 0.1 M NaOH solution in a water and ethanol mixture (1:1, v/v) and measured the concentration of desorbed dye by a Perkin-Elmer UV−vis spectrophotometer (model Lambda 950). The diffusereflectance spectra of the TiO_2 films were recorded on the same UV−vis spectrophotometer at the same time.

■ RESULTS AND DISCUSSION

Figure 1(a−c), as a series of representative field emission scanning electron microscopy (FESEM) images, clearly show the core−shell structure of the as-prepared TiO_2. Figure 1(a) is a panoramic image of the obtained product. The sample was mainly composed of uniform and well-dispersed microspheres. A high-magnification FE-SEM image (Figure 1(b)) reveals that the surface of the TiO_2 microspheres is rough. The external shells of the microspheres consist of uniform nanopolyhedra, which can be clearly observed from the white square area. It was reported that the surface fluorination can dramatically reduce the (001)-faceted surface energy to a level lower than that of the (101) facet, producing anatase TiO_2 single crystals exposed with more (001) facets.[25] According to the symmetries of anatase TiO_2 crystals, the two flat and square surfaces should be (001) facets, and the eight quadrilateral surfaces should be (101) facets of these crystals.[26,28] Thus, the (101) and (001) crystal facets of the single nanopolyhedra were marked out in the white square area of Figure 1B. The unique core–shell nanostructures can be seen more clearly from an individual broken TiO_2 microsphere in Figure 1(c). The typical diameter of these microspheres is about 600 nm. The external shells consist of ~80 nm TiO_2 nanopolyhedra, while the interior sphere is composed of smaller spherical nanoparticles having sizes between 30–40 nm. Figure 1(d) shows the X-ray diffraction (XRD) patterns for TiO_2 spheres, indicating that sample possesses highly crystallized anatase without any other phases. The strong and sharp diffraction peaks indicate the good crystallinity of the as-prepared products.

The morphology and structure of the as-synthesized core–shell TiO_2 micro-nanostructure are further characterized by HRTEM and are shown in Figure 2. Figure 2(a) shows the overall view of the core–shell MTM. The dark center and bright edge of the TiO_2 spheres reveal the core–shell nature of the sample. Figure 2(b) shows the high-magnification TEM image of the TiO_2 polyhedra in the surface of the core–shell microsphere. TEM images of the as-synthesized products clearly show that the TiO_2 spheres shell consists of flat nanopolyhedra, and the mesoporous structure in the flat nanopolyhedra are clearly shown. The white square area in Figure 2(b) is further magnified and is shown in Figure 2(c). The pore diameter is about 4 nm. The HRTEM image of the irregularly mesoporous structure was further investigated and is shown in Figure 2(d). It is clear that the mesopore is irregular, which indicates that the pore is not formed by a regular template. The formation of the mesopore may be due to the anisotropic etching by HF, which is generated in the reaction process (see below for details). The lattice distance of the fine fringes is about 0.35 nm, which corresponds to the (001) plane of the anatase TiO_2.

To further research into the porous structure and pore size distribution of the as-obtained products, nitrogen adsorption–desorption isotherms are measured to ascertain the specific surface area and pore size of the TiO_2 microspheres. As shown in Figure 3, the nitrogen adsorption–desorption isotherm belongs to type IV, and the hysteresis loop observed in these isotherms is indicative of the existence of mesoporous structures in the architectures according to the IUPAC classification. The plot of the pore diameter distribution was determined by using the Barrett–Joyner–Halenda (BJH) method from the desorption branch of the isotherm (inset, Figure 3). The peak pore is about 4.19 nm, which fits with the TEM image. The BET surface area of the TiO_2 microspheres is 33.6 m^2/g.

The mechanism for the formation of our core–shell-structured MTMs would be speculated as follows. Before we suppose the formation mechanism, we list all the chemical reactions that could be involved in our synthetic process. The possible reactions responsible for the formation of the core–shell-structured MTMs in the presence of hydrogen peroxide and ammonium fluoride are listed as follows:

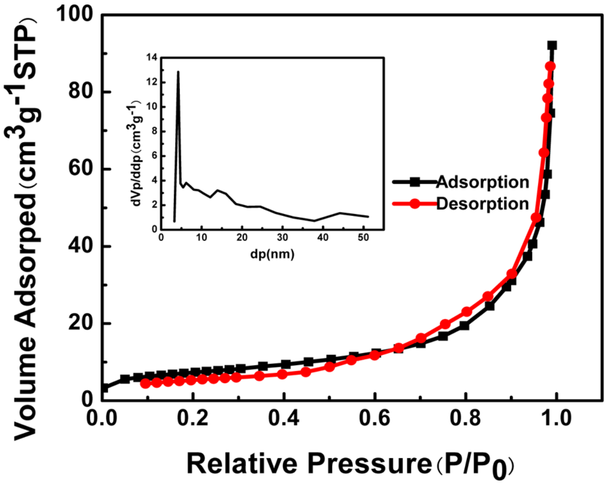

Figure 3. Nitrogen adsorption–desorption isotherm and corresponding Barrett–Joyner–Halenda (BJH) pore size distribution curve (inset) of the MTM.

$$Ti^{4+} + H_2O_2 \rightarrow Ti(O_2)^{2+} + 2H^+ \qquad (1)$$

$$Ti(O_2)^{2+} + 2H_2O \rightarrow 2TiO_2 + O_2 + 4H^+ \qquad (2)$$

$$NH_4F + H_2O \rightarrow NH_3{\cdot}H_2O + HF \qquad (3)$$

$$TiO_2 + 4HF \rightarrow TiF_4 + 2H_2O \qquad (4)$$

$$TiF_4 + 2H_2O \rightarrow TiO_2 + 4HF \qquad (5)$$

In the hydrothermal process, the oxygen bubbles produced by the decomposition of $Ti(O_2)^{2+}$ can act as soft templates for the formation of core–shell-structured MTMs.[34] NH_4F is crucial for the (001) facets erosion of the microsphere shells and for controlling the crystal morphology of microsphere shells. It is proposed that the F ion can interact strongly with the (001) facets, reducing the surface energy and kinetically inhibiting crystal growth, which favors the formation of (001) facets,[35] resulting in anatase TiO_2 flat polyhedra with two highly exposed (001) facets and eight (101) facets.[36] On the basis of our previous investigation, we proposed an anisotropic corrosion mechanism[31] for the formation of the core–shell-structured TiO_2 microsphere sample with a mesoporous structure on (001) facets. As depicted in Scheme 1, in the beginning of the reaction, the white TiO_2 precursor dissolved to form TiO_2 nanoparticles. The Ti/F ratio is very high, and the rate of crystallization of TiO_2 under hydrothermal conditions is fast.[37,38] These crystalline TiO_2 nanoparticles will aggregate around the gas–liquid interface of the O_2 bubbles. The internal titanium dioxide spherical particles with a higher surface energy and a smaller diameter would dissolve and transfer to the external flat nanocrystal in the microsphere shell and redeposit and recrystallize on the better crystallized TiO_2 nanoparticles of the shell[39] (step 2, Scheme 1). During this period, F ions are mainly absorbed onto the (001) facets of TiO_2 particles, leading to a lower surface free energy than that of the (101) surfaces, which actually promotes the growth of anatase crystallite in the [001] direction, and thus, the head-truncated anatase TiO_2 polyhedra appeared. At the last stage, however, the selective

Scheme 1. Schematic Representation of the Formation Mechanism of the Core–Shell-Structured TiO_2 Microsphere

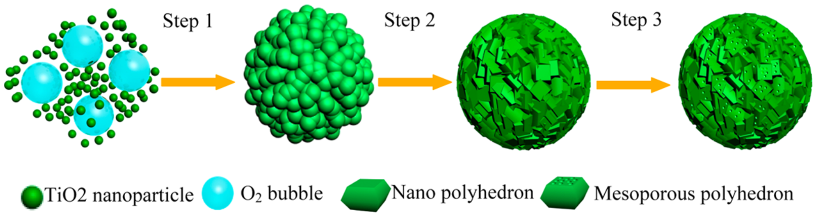

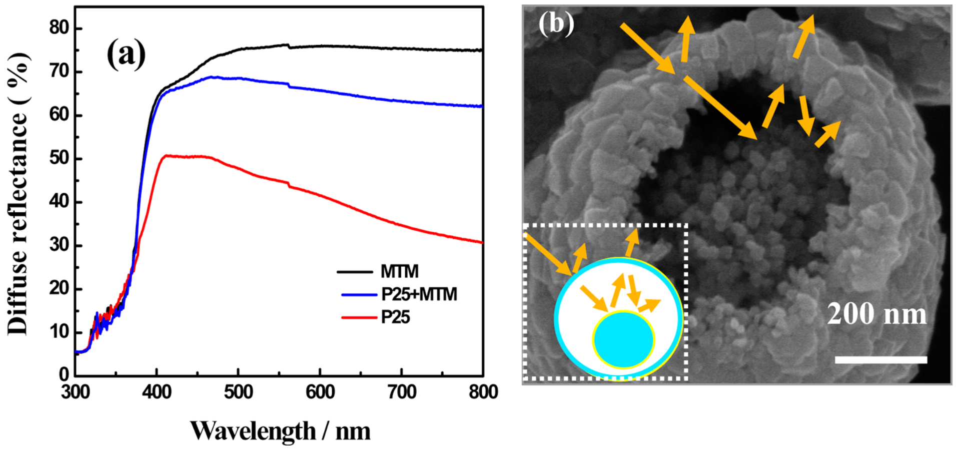

Figure 4. (a) UV–vis diffuse reflectance spectra of the three types of films. (b) Schematic illustration of multi-reflections within the core–shell-structured MTM.

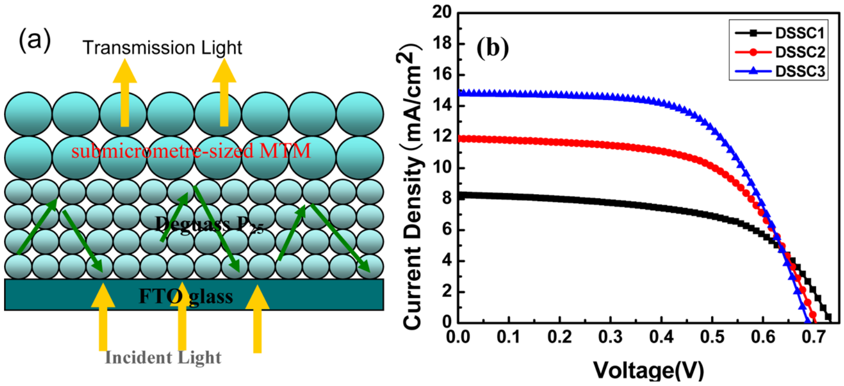

Figure 5. (a) Schematic illustration of the scattering layer using the core–shell structure of the as-prepared product. (b) *I*–*V* characteristics of the produced DSSCs.

chemical etching of F^- on (001) facets occurs because most of the Ti ions have been consumed to build the particle, and hence, the Ti/F ratio is very low.[37,40] When all titanium ions were depleted, the excessive corrosive HF started to act as an etching agent for the (001) facet of the TiO_2 pyramids and left (101) facets unetched along the [001] direction. Because of the concentration gradient of HF along the corrosion direction, tapered holes were created in the shell of the nanoparticles. Finally, a mesoporous structure was formed in the surface of the TiO_2 flat pyramids and left (101) facets with low surface energy unetched (step 3, Scheme 1).

The high light-scattering ability of the TiO_2 electrode is important for improving the light-harvesting efficiency and thus photon-to-current conversion efficiency of the resulting DSSC. Figure 4(a) shows the diffuse reflectance spectra of the three types of TiO_2 films in the range of visible light. All three films have high diffuse reflection capacities in the short wavelength range (400–475 nm), while the diffuse reflectance of the P_{25} film is descending more rapid than that of the other two films in the wavelength range between 475 and 800 nm. Compared to the P_{25} TiO_2 films, the films composed of light-scattering and transparent layers (P_{25} + MTMs) had higher diffuse reflection capabilities in the visible and near-infrared regions (450–800 nm), indicating that the incident light was significantly scattered within the film because of the introduction of submicrometer-sized MTMs. The core–shell structures are composed of nanocrystallites to form large secondary particles, thereby functioning as a light-scattering layer. Figure 4(b) shows the schematic illustration of multi-reflections within the core–shell-structured MTM. It is obvious that the core–shell structures microspheres are composed of mesoporous single-crystal TiO_2 nanopolyhedra with highly exposed (001) facets and are favorable for multi-reflecting of light.

This paper reports the use of the transparent high surface area Degussa P_{25} layers and scattering layer comprising of relatively larger as-prepared product, thus ensuring adequate light trapping in these devices. Because of the extremely large particle sizes and special core−shell structure of the as-prepared product, it functions as a light-scattering layer. The additional light-scattering layer ensures capture of the light into the device, which otherwise will be lost due to the transparency of the P_{25} layers (Figure 5). The as-prepared product and P_{25} respectively form the light-scattering and transparent layers of the photoanode. we refer to this DSSC as DSSC-3, the one based on P_{25} as DSSC-2, and the one based on our as-prepared sample as DSSC-1.

The characteristic current−voltage (I−V) curves are shown in Figure 5. Values of other parameters, for example, short-circuit current density (J_{sc}), open circuit voltage (V_{oc}), fill factor (FF), and overall current conversion efficiency (η) of the tested DSSCs, are listed in Table 1. We notice that DSSC-3 displayed a higher J_{sc} of 14.94 mA/cm2 and η of 6.42%, corresponding to the 25% and 21% increments in comparison with those based on the P_{25} electrode (DSSC-2), while the V_{oc} remained much the same as that of P_{25}. In order to understand how these factors play roles in affecting the performance of our DSSCs devices, we carried out dye adsorption measurements of the three photoanodes. The dye absorption amount in DSSC-3 was 1.22×10^{-7} mol cm^{-2}, which was lower than that of DSSC-2, which was as high as 1.87×10^{-7} mol cm^{-2}. Thus, the superior photoelectric conversion efficiency of DSSC-3 could be explained by better light utilization efficiency, which compensates for the inferior dye adsorption. Furthermore, the dye loading of DSSC-1 was 1.13×10^{-7} mol cm^{-2}, a comparable value with DSSC-3, and showed the minimal light to electricity conversion efficiency. The greater light loss in the photoanode of DSSC-1 caused by the strong light-scattering layer with the lack of a conventional photoactive layer should be the reason for low conversion efficiency. Besides, the core−shell-structured MTM-based DSSCs showed a rather high amount of dye adsorption, which may be attributed to both the massive exposed (101) facets with a strong ability to absorb dye molecules and the mesoporous structure that is a well-known structure for dye adsorption. We can conclude that the amount of dye adsorption was not the main factor that affected the performance of our DSSCs devices; the strong light-scattering effect from the core−shell-structured anatase TiO_2 promotes cell performance.

Table 1. Characterized Results for the Three DSSCs

prepared cells	V_{oc} (V)	J_{sc} (mA/cm^2)	FF (%)	η (%)	C ($\times 10^{-7}$ mol cm^{-2})
DSSC-1	0.73	8.3	59	3.6	1.1
DSSC-2	0.70	11.9	61	5.1	1.9
DSSC-3	0.70	14.9	62	6.6	1.2

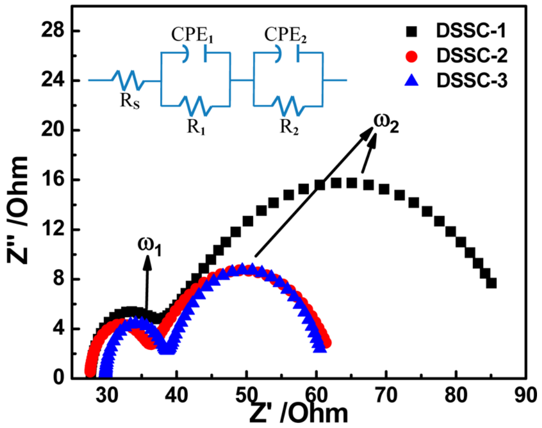

Figure 6. Nyquist spectra of the three DSSCs.

To reveal the internal resistances of the cells, the Nyquist plots of the three cells were obtained in the frequency range from 10^0 to 10^5 Hz at the applied bias of V_{oc} under AM 1.5 G one sun illumination. The electrochemical impedance spectroscopy[41] results were fitted by the equivalent circuit (inset, Figure 6) using ZsimpWin software. In general, the small semicircle in the high-frequency region (ω_1) mainly reflects the electron transfer resistance at the electrolyte/Pt-FTO interface, while the large semicircle in the low-frequency region (ω_2) represents the resistance of electron transportation at the photoanode/electrolyte interface.[42,43] From the plots in Figure 6, we can see that DSSC-1 showed the largest semicircles among the three DSSCs in both high-frequency and low-frequency regions, which is mainly due to the relatively larger size of the obtained TiO_2 core−shell-structured MTMs and hence the weak electric contact of the as-prepared product.[44] After the introduction of the P_{25} paste, which serves as the sublayer, the multi-layer DSSC-3 photoanode showed a smaller semicircle at frequency region ω_2 compared with the DSSC based on the P_{25} photoanode; the fitted resistance values are 20.2 and 23.3 Ω, respectively. The reduced interfacial electron transfer resistance could be explained by the synergistic effect of P_{25} with a high amount of dye adsorption and the submicrometer-sized core−shell-structured MTMs with excellent light-scattering; both contribute to the high electron density within the photoanode. In summary, the DSSC-3 with smaller essential resistance indicates that the as-prepared core−shell-structured MTMs are suitable for constructing a high efficiency photoanode.

To conclude, core−shell-structured MTMs were synthesized via a hydrothermal synthesis method. The obtained mesoporous TiO_2 core−shell-structured MTMs possess rather high surface areas and microsphere shells with highly exposed (101) facets, and both of them are favorable for dye adsorption. The cooperative light-scattering effect of the unique core−shell-structured anatase TiO_2 and the single-crystal TiO_2 nanopolyhedra promotes cell performance.

■ CONCLUSIONS

In summary, a simple one-step hydrothermal synthesis method has been developed to prepare complicated structures of mesoporous sphere-in-shell anatase TiO_2 microspheres. We prepared the photoanode using Degussa P_{25} as the transparent layers and a relatively larger as-prepared product as the scattering layer, ensuring adequate light trapping in these devices. The relatively large particle sizes and special core−shell structure of the as-prepared product ensures capture of the radiation into the device. The DSSCs with an additional scattering layer showed an overall light-to-electricity conversion efficiency of 6.64%, achieving a 27% increase in the conversion efficiency compared to the standard Degussa P_{25} photoanode.

■ AUTHOR INFORMATION

Corresponding Author

*Tel: +86-25-83172270. Fax: +86-25-83172270. E-mail address: Zhouxf@njtech.edu.cn.

Notes

The authors declare no competing financial interest.

ACKNOWLEDGMENTS

This research was supported by the Natural Science Foundation of China (U1162108 and 51272104), Natural Science Foundation of Jiangsu Province Office of Education (11KJA150002 and 10KJB150006), Financial Foundation of State Key Laboratory of Materials-Oriented Chemical Engineering, and A Project Funded by the Priority Academic Program Development of Jiangsu Higher Education Institutions.

REFERENCES

(1) Law, M.; Greene, L. E.; Johnson, J. C.; Saykally, R.; Yang, P. Nanowire dye-sensitized solar cells. *Nat. Mater.* **2005**, *4* (6), 455−459.

(2) Tu, L.; Pan, H.; Xie, H.; Yu, A.; Xu, M.; Chai, Q.; Cui, Y.; Zhou, X. Study on the fabrication and photovoltaic property of TiO_2 mesoporous microspheres. *Solid. State. Sci.* **2012**, *14* (5), 616−621.

(3) Wang, M.; Moon, S. J.; Xu, M.; Chittibabu, K.; Wang, P.; Cevey-Ha, N. L.; Humphry - Baker, R.; Zakeeruddin, S. M.; Grätzel, M. Efficient and stable solid-state dye-sensitized solar cells based on a high molar extinction coefficient sensitizer. *Small* **2010**, *6* (2), 319−324.

(4) Zhang, L.; Jihuai, W. Recent progress in flexible dye-sensitized solar cells. *Prog. Chem.* **2010**, *22* (11), 2248−2253.

(5) Zhang, Q.; Dandeneau, C. S.; Zhou, X.; Cao, G. ZnO nanostructures for dye-sensitized solar cells. *Adv. Mater.* **2009**, *21* (41), 4087−4108.

(6) Szeifert, J. M.; Feckl, J. M.; Fattakhova-Rohlfing, D.; Liu, Y.; Kalousek, V.; Rathousky, J.; Bein, T. Ultrasmall titania nanocrystals and their direct assembly into mesoporous structures showing fast lithium insertion. *J. Am. Chem. Soc.* **2010**, *132* (36), 12605−12611.

(7) Tang, Y.-B.; Lee, C.-S.; Xu, J.; Liu, Z.-T.; Chen, Z.-H.; He, Z.; Cao, Y.-L.; Yuan, G.; Song, H.; Chen, L. Incorporation of graphenes in nanostructured TiO_2 films via molecular grafting for dye-sensitized solar cell application. *Acs. Nano* **2010**, *4* (6), 3482−3488.

(8) Mor, G. K.; Varghese, O. K.; Paulose, M.; Shankar, K.; Grimes, C. A. A review on highly ordered, vertically oriented TiO_2 nanotube arrays: Fabrication, material properties, and solar energy applications. *Sol. Energy Mater. Sol. Cells* **2006**, *90* (14), 2011−2075.

(9) Zheng, H.; Tachibana, Y.; Kalantar-zadeh, K. Dye-sensitized solar cells based on WO_3. *Langmuir* **2010**, *26* (24), 19148−19152.

(10) Quintana, M.; Edvinsson, T.; Hagfeldt, A.; Boschloo, G. Comparison of dye-sensitized ZnO and TiO_2 solar cells: Studies of charge transport and carrier lifetime. *J. Phys. Chem. C* **2007**, *111* (2), 1035−1041.

(11) Tan, B.; Wu, Y. Dye-sensitized solar cells based on anatase TiO_2 nanoparticle/nanowire composites. *J. Phys. Chem. B* **2006**, *110* (32), 15932−15938.

(12) Liu, B.; Aydil, E. S. Growth of oriented single-crystalline rutile TiO_2 nanorods on transparent conducting substrates for dye-sensitized solar cells. *J. Am. Chem. Soc.* **2009**, *131* (11), 3985−3990.

(13) Jiu, J.; Isoda, S.; Wang, F.; Adachi, M. Dye-sensitized solar cells based on a single-crystalline TiO_2 nanorod film. *J. Phys. Chem. B* **2006**, *110* (5), 2087−2092.

(14) Chen, C.-C.; Chung, H.-W.; Chen, C.-H.; Lu, H.-P.; Lan, C.-M.; Chen, S.-F.; Luo, L.; Hung, C.-S.; Diau, E. W.-G. Fabrication and characterization of anodic titanium oxide nanotube arrays of controlled length for highly efficient dye-sensitized solar cells. *J. Phys. Chem. C* **2008**, *112* (48), 19151−19157.

(15) Shankar, K.; Mor, G. K.; Prakasam, H. E.; Varghese, O. K.; Grimes, C. A. Self-assembled hybrid polymer-TiO_2 nanotube array heterojunction solar cells. *Langmuir* **2007**, *23* (24), 12445−12449.

(16) Roy, P.; Kim, D.; Lee, K.; Spiecker, E.; Schmuki, P. TiO_2 nanotubes and their application in dye-sensitized solar cells. *Nanoscale* **2010**, *2* (1), 45−59.

(17) Feng, X.; Shankar, K.; Varghese, O. K.; Paulose, M.; Latempa, T. J.; Grimes, C. A. Vertically aligned single crystal TiO_2 nanowire arrays grown directly on transparent conducting oxide coated glass: synthesis details and applications. *Nano Lett.* **2008**, *8* (11), 3781−3786.

(18) Liao, J.-Y.; Lei, B.-X.; Chen, H.-Y.; Kuang, D.-B.; Su, C.-Y. Oriented hierarchical single crystalline anatase TiO_2 nanowire arrays on Ti-foil substrate for efficient flexible dye-sensitized solar cells. *Energy Environ. Sci.* **2012**, *5* (2), 5750−5757.

(19) Tao, R.-H.; Wu, J.-M.; Xue, H.-X.; Song, X.-M.; Pan, X.; Fang, X.-Q.; Fang, X.-D.; Dai, S.-Y. A novel approach to titania nanowire arrays as photoanodes of back-illuminated dye-sensitized solar cells. *J. Power Sources* **2010**, *195* (9), 2989−2995.

(20) Zukalova, M.; Zukal, A.; Kavan, L.; Nazeeruddin, M. K.; Liska, P.; Grätzel, M. Organized mesoporous TiO_2 films exhibiting greatly enhanced performance in dye-sensitized solar cells. *Nano Lett.* **2005**, *5* (9), 1789−1792.

(21) Koops, S. E.; O'Regan, B. C.; Barnes, P. R.; Durrant, J. R. Parameters influencing the efficiency of electron injection in dye-sensitized solar cells. *J. Am. Chem. Soc.* **2009**, *131* (13), 4808−4818.

(22) Hou, K.; Tian, B.; Li, F.; Bian, Z.; Zhao, D.; Huang, C. Highly crystallized mesoporous TiO_2 films and their applications in dye sensitized solar cells. *J. Mater. Chem.* **2005**, *15* (24), 2414−2420.

(23) Chen, D.; Huang, F.; Cheng, Y. B.; Caruso, R. A. Mesoporous anatase TiO_2 beads with high surface areas and controllable pore sizes: A superior candidate for high-performance dye-sensitized solar cells. *Adv. Mater.* **2009**, *21* (21), 2206−2210.

(24) Koo, H. J.; Kim, Y. J.; Lee, Y. H.; Lee, W. I.; Kim, K.; Park, N. G. Nano-embossed hollow spherical TiO_2 as bifunctional material for high-efficiency dye-sensitized solar cells. *Adv. Mater.* **2008**, *20* (1), 195−199.

(25) Park, N.-G.; Van de Lagemaat, J.; Frank, A. Comparison of dye-sensitized rutile- and anatase-based TiO_2 solar cells. *J. Phys. Chem. B* **2000**, *104* (38), 8989−8994.

(26) Banfield, J. Thermodynamic analysis of phase stability of nanocrystalline titania. *J. Mater. Chem.* **1998**, *8* (9), 2073−2076.

(27) Liu, M.; Piao, L.; Zhao, L.; Ju, S.; Yan, Z.; He, T.; Zhou, C.; Wang, W. Anatase TiO_2 single crystals with exposed {001} and {110} facets: Facile synthesis and enhanced photocatalysis. *Chem. Commun.* **2010**, *46* (10), 1664−1666.

(28) Diebold, U. The surface science of titanium dioxide. *Surf. Sci. Rep.* **2003**, *48* (5), 53−229.

(29) Adachi, M.; Murata, Y.; Takao, J.; Jiu, J.; Sakamoto, M.; Wang, F. Highly efficient dye-sensitized solar cells with a titania thin-film electrode composed of a network structure of single-crystal-like TiO_2 nanowires made by the "oriented attachment" mechanism. *J. Am. Chem. Soc.* **2004**, *126* (45), 14943−14949.

(30) Crossland, E. J.; Noel, N.; Sivaram, V.; Leijtens, T.; Alexander-Webber, J. A.; Snaith, H. J. Mesoporous TiO_2 single crystals delivering enhanced mobility and optoelectronic device performance. *Nature* **2013**, *495* (7440), 215−219.

(31) Liu, L.; Qian, J.; Li, B.; Cui, Y.; Zhou, X.; Guo, X.; Ding, W. Fabrication of rutile TiO_2 tapered nanotubes with rectangular cross-sections via anisotropic corrosion route. *Chem. Commun.* **2010**, *46* (14), 2402−2404.

(32) Yu, J.; Zhang, J. A simple template-free approach to TiO_2 hollow spheres with enhanced photocatalytic activity. *Dalton Trans.* **2010**, *39* (25), 5860−5867.

(33) Yue, W.; Xu, X.; Irvine, J. T.; Attidekou, P. S.; Liu, C.; He, H.; Zhao, D.; Zhou, W. Mesoporous monocrystalline TiO_2 and its solid-state electrochemical properties. *Chem. Mater.* **2009**, *21* (12), 2540−2546.

(34) Lu, J.; Bauermann, L. P.; Gerstel, P.; Heinrichs, U.; Kopold, P.; Bill, J.; Aldinger, F. Synthesis and characterization of TiO_2 nano-powders from peroxotitanium solutions. *Mater. Chem. Phys.* **2009**, *115* (1), 142−146.

(35) Liu, S.; Yu, J.; Jaroniec, M. Tunable photocatalytic selectivity of hollow TiO_2 microspheres composed of anatase polyhedra with exposed {001} facets. *J. Am. Chem. Soc.* **2010**, *132* (34), 11914−11916.

(36) Yang, H. G.; Sun, C. H.; Qiao, S. Z.; Zou, J.; Liu, G.; Smith, S. C.; Cheng, H. M.; Lu, G. Q. Anatase TiO_2 single crystals with a large percentage of reactive facets. *Nature* **2008**, *453* (7195), 638−641.

(37) Pan, L.; Zou, J.-J.; Wang, S.; Liu, X.-Y.; Zhang, X.; Wang, L. Morphology evolution of TiO_2 facets and vital influences on photocatalytic activity. *ACS Appl. Mater. Interfaces* **2012**, *4* (3), 1650−1655.

(38) Yu, J.; Zhang, J. A simple template-free approach to TiO_2 hollow spheres with enhanced photocatalytic activity. *Dalton Trans.* **2010**, *39* (25), 5860−5867.

(39) Cui, Y.; Liu, L.; Li, B.; Zhou, X.; Xu, N. Fabrication of tunable core−shell structured TiO_2 mesoporous microspheres using linear polymer polyethylene glycol as templates. *J. Phys. Chem. C* **2010**, *114* (6), 2434−2439.

(40) Lei, L.; Yuming, C.; Bo, L.; Xingfu, Z.; Weiping, D. Study on the surface erosion route to the fabrication of TiO_2 hollow spheres. *Appl. Surf. Sci.* **2010**, *256* (8), 2596−2601.

(41) Magne, C.; Dufour, F.; Labat, F.; Lancel, G.; Durupthy, O.; Cassaignon, S.; Pauporté, T. Effects of TiO_2 nanoparticle polymorphism on dye-sensitized solar cell photovoltaic properties. *J. Photochem. Photobiol. A* **2012**, *232*, 22−31.

(42) Feng, X.; Shankar, K.; Paulose, M.; Grimes, C. A. Tantalum-doped titanium dioxide nanowire arrays for dye-sensitized solar cells with high open-circuit voltage. *Angew. Chem., Int. Ed.* **2009**, *121* (43), 8239−8242.

(43) Van de Lagemaat, J.; Park, N.-G.; Frank, A. Influence of electrical potential distribution, charge transport, and recombination on the photopotential and photocurrent conversion efficiency of dye-sensitized nanocrystalline TiO_2 solar cells: A study by electrical impedance and optical modulation techniques. *J. Phys. Chem. B* **2000**, *104* (9), 2044−2052.

(44) Adachi, M.; Sakamoto, M.; Jiu, J.; Ogata, Y.; Isoda, S. Determination of parameters of electron transport in dye-sensitized solar cells using electrochemical impedance spectroscopy. *J. Phys. Chem. B* **2006**, *110* (28), 13872−13880.